# A New Railway Power Flow Control System Coupled With Asymmetric Double *LC* Branches

Sijia Hu, *Student Member, IEEE*, Zhiwen Zhang, Yong Li, *Senior Member, IEEE*, Longfu Luo, *Member, IEEE*, Pei Luo, Yijia Cao, *Senior Member, IEEE*, Yuehui Chen, Guandong Zhou, Bin Wu, *Fellow, IEEE*, and Christian Rehtanz, *Senior Member, IEEE*

***Abstract*—Facing the challenges of power quality problems and excessive neutral sections of conventional two-phase electric railway supply system, the way of adopting railway static power conditioner (RPC)-based single-phase supply system is a feasible solution. To enhance the cost-efficiency and reliability of RPC, a novel compensating system named asymmetric double *LC*-coupled railway power flow conditioner (ALC-RPFC) is proposed in this paper. The study indicates that compared with the conventional RPC, the proposed ALC-RPFC has an effective heavy-load compensating ability with lower power rating, which is benefit to enhance converter's operating efficiency and reliability. Besides, a design method for *LC* coupling branches mentioned in this paper is suitable for fluctuated railway loads, and is useful for designers of industrial applications as well. Finally, the good heavy-load compensating performance and power capacity decreasing ability of the ALC-RPFC are validated based on simulation and experiment results.**

***Index Terms*—Asymmetric *LC*-coupling branches, electrical railway power system, parameter design, power capacity analysis, power flow control.**

## I. Introduction

With the wide application of high-speed and heavy-load trains in railway networks, the negative sequence current (NSC), reactive power, and harmonics injected into the power grids increase significantly, which seriously affects the stability of utility, and arouses widespread attention of related industrial departments and engineers [1]–[3].

Manuscript received March 24, 2014; revised June 23, 2014, August 7, 2014, and September 21, 2014; accepted October 27, 2014. Date of publication November 10, 2014; date of current version May 22, 2015. This work was supported in part by the NSFC under Grants 51477046 and 51377001, the National Science and Technology Support Program of China under Grant 2013BAA01B01, the Hunan Province Innovation Foundation for Postgraduate under Grant CX2014B131, the Key Project of Hunan Provincial Natural Science Foundation of China under Grant 12JJ2034, and the Science and Technology Program of China State Grid under Grant 5216A0140002. Recommended for publication by Associate Editor D. Vinnikov.

S. Hu, Z. Zhang, Y. Li, L. Luo, P. Luo, and Y. Cao are with the College of Electrical and Information Engineering, Hunan University, Changsha 410082, China (e-mail: huda_hsj@163.com; zzw@126.com; yonglichi@gmail.com; llf@hnu.edu.cn; Lpmq@163.com; yjcao@hnu.edu.cn).

Y. Chen and G. Zhou are with the State Grid Hunan Electric Power Company, Changsha 410007, China (e-mail: chenyh6@hn.sgcc.com.cn; zhougd@hn.sgcc.com.cn).

B. Wu is with the Department of Electrical and Computer Engineering, Ryerson University, Toronto, ON M5B 2K3, Canada (e-mail: bwu@ee.ryerson.ca).

C. Rehtanz is with the Institute of Energy Systems, Energy Efficiency and Energy Economics, TU Dortmund, Dortmund 44227, Germany (e-mail: christian.rehtanz@tu-dortmund.de).

Color versions of one or more of the figures in this paper are available online at http://ieeexplore.ieee.org.

Digital Object Identifier 10.1109/TPEL.2014.2369132

Considering the efficiency, adoption of the phase rotation technique is the most conventional method for electrical railway power system [4]. However, it lacks flexibility and cannot solve all power quality problems. Moreover, these problems will become more prominent in the remote areas with unrobust power system (e.g., mountainous and plateaus areas).

Compared to conventional transformers, the balance traction transformer (BTT) can have a better ability of suppressing NSC. Unfortunately, the ability of BTT to suppress NSC is affected by load variation. That is to say, the greater imbalance of two-phase loads, the worse ability of NSC suppression [5], [6]. Therefore, the three-phase power system can hardly be balanced by this method. Besides, this class of special-type transformer usually contains a complex winding structure, and it is also not beneficial for the elimination of harmonics and reactive power.

SCR-controlled static VAR compensator can also be used to compensate NSC and reactive power in traction supply systems. But it is difficult to get a satisfactory state in both technical and economic aspects [7].

To overcome the disadvantages, various IGBT- or IGCT-based active compensating systems were put forward in the last 20 years [8]–[21]. Among them, RPC gets more attention due to its universalness [17]–[21]. It can deal with almost all power quality problems of two-phase and single-phase traction supply system. However, a relatively high compensation capacity and initial investment slow down its large-scale industrial application. Additionally, a high operating voltage (or dc-link voltage) of the converters is necessary. RPC has been used in a few traction substations (TSSs) of China and Japan since it was first proposed in 1993 [18]–[20].

Currently, the research on low-rated power conditioners is focused on hybrid active filters [22]–[25] and unified power quality conditioners [26]–[27]. Unfortunately, there is still few research related to the field of hybrid power conditioner for electrical railway power system. Two main reasons make it difficult to design the coupling passive elements of these conditioners: 1) the railway loads usually change rapidly within few seconds in real traction supply system (see Fig. 15 in Section VI), the complex working condition of locomotives make it difficult to estimate; 2) the power quality controllers should have the ability of comprehensive compensating NSC, reactive power, and harmonics in the same time with relatively low power rating. To the authors' knowledge, [9] proposed a useful configuration; [12], [14], and [15] discussed just one side of the three basic requirements stated previously, while some other researches are still analyzed, designed, and verified based on a static working

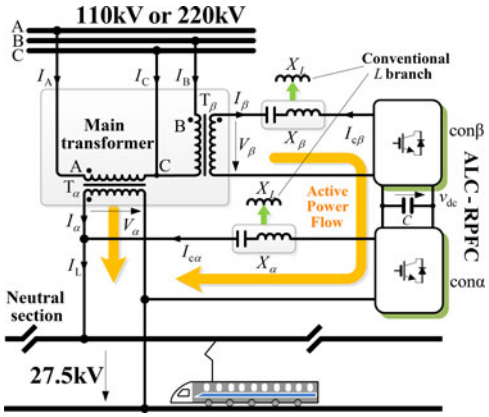


Fig. 1. Topology of ALC-RFPC system.

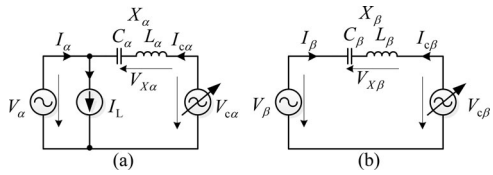


Fig. 2. Equivalent circuits of phase-$\alpha$ and $\beta$. (a) Phase-$\alpha$. (b) Phase-$\beta$.

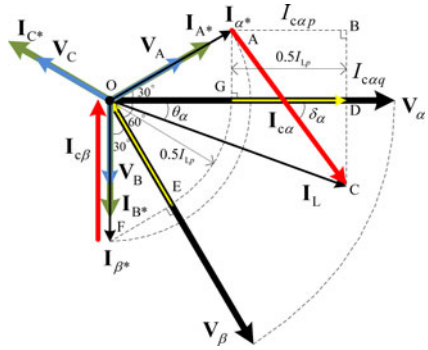

Fig. 3. Compensating phasor diagram of ALC-RPFC system.

situation, which their industrial application value is limited and suspected significantly in real electrical railway power systems [21].

To overcome these problems, a new topology, ALC-RPFC, and the corresponding design method of the passive elements under load fluctuated working condition are proposed in this paper. As shown in Fig. 1, ALC-RPFC is mainly composed of two simple single-phase transformers and a back-to-back converter. Because the coupling parts between feeders and converters are two different *LC*-branches, we named it as asymmetric double *LC*-coupled railway power flow conditioner (i.e., ALC-RPFC); whereas the conventional RPC consists of two symmetric L-branches. The main purpose of this paper is to propose a systematic design method of the *LC* branches and the corresponding power capacity quantitative analysis method, which is suitable for the fluctuated electrical railway loads.

In the following, the topology of ALC-RPFC will be discussed in Section II. In Section III, the converter's operating performance is analyzed. The main contribution of this paper on the load variation based design method of *LC*-branches and the power capacity analysis will be given in Sections IV and V, respectively. Section VI gives the results of simulation and experiment. Finally, the conclusion is given in Section VII.

## II. Topology of ALC-RPFC System

Fig. 1 shows the topology of ALC-RPFC system. The three phase 110 kV (or 220 kV) high voltage grid is stepped down into 27.5-kV single-phase traction network by $\mathrm{T}_\alpha$ so as to feed locomotives. While $\mathrm{T}_\beta$'s secondary voltage, $V_\beta$, is not always 27.5 kV, its design value depends on the load's statistical results (see Section IV). Two power converters, con$\alpha$ and con$\beta$, back to back connection; through two *LC* branches, $X_\alpha$ and $X_\beta$, they are coupled with the main transformer, respectively.

Besides, multilevel topology can also be used in this conditioner, which can eliminate the need of two auxiliary bulky low frequency step-down transformers [9] (Note that the dc bus in this topology may not be unique [28].).

Fig. 2 shows the equivalent circuit of phase-$\alpha$ and $\beta$. Among which, $V_{ck}$ and $I_{ck}$ are the fundamental voltage and current of converter k, respectively; $X_k$ is the equivalent fundamental reactance and $V_{X\,k}$ the voltage drop of coupling branch in phase k, respectively; $V_k$ and $I_k$ are the secondary voltage and current of $\mathrm{T}_k$; $I_L$ is the load's current ($k \in \{\alpha, \beta\}$).

## III. Operating Property of ALC-RPFC

### A. Basic Requirements of Converters

Ignoring the influences of harmonics and turn's ratio difference between $\mathrm{T}_\alpha$ with $\mathrm{T}_\beta$; the phasor diagram of ALC-RPFC is shown in Fig. 3 (Note that the voltages and currents of phase-$\beta$ shown in Fig. 3 are converted to the same level of phase-$\alpha$.). ALC-RPFC should satisfy the following requirements [17]:

1) Transforming half of the load's active power from phase-$\beta$ (EO, i.e., $0.5I_{Lp}$) to phase-$\alpha$ (GD, i.e., $0.5I_{Lp}$).
2) Compensating appropriate leading reactive power for phase-$\alpha$ (BC) and lagging reactive power for phase-$\beta$ (EF).

Therefore, it can be observed from Fig. 3 that the output currents of $\mathrm{T}_\alpha$ and $\mathrm{T}_\beta$ are converted from $\mathbf{I}_\mathrm{L}$ and $\mathbf{0}$ into $\mathbf{I}_{\alpha*}$ and $\mathbf{I}_{\beta*}$, respectively. The primary three phase currents $\mathbf{I}_{\mathrm{A}*}$, $\mathbf{I}_{\mathrm{B}*}$, and $\mathbf{I}_{\mathrm{C}*}$ inducted by $\mathbf{I}_{\alpha*}$ and $\mathbf{I}_{\beta*}$ are balanced as well. Obviously, their PF is 1. Hence, the compensation currents of con$\alpha$ and con$\beta$ are $\mathbf{I}_{c\alpha}$ and $\mathbf{I}_{c\beta}$, respectively. By the way, this compensating principle is also useful for RPC [17].

To get the requirements stated previously, referring to Fig. 3, $\delta_\alpha\,(\delta_\alpha = \angle\mathbf{V}_\alpha - \angle\mathbf{I}_{c\alpha})$ and the load's PF, $\lambda(\lambda = cos\theta_\alpha)$, should satisfy

$$\delta_\alpha = \arctan\left(\frac{|I_{c\alpha q}|}{|I_{c\alpha p}|}\right) = \arctan\left(\frac{1}{\sqrt{3}} + 2\sqrt{\frac{1}{\lambda^2} - 1}\right) \quad (1)$$

where $I_{c\alpha p}$ and $I_{c\alpha q}$ are the active and reactive part of $\mathbf{I}_{c\alpha}$, respectively (i.e., AB and BC in Fig. 3). From (1), the relationship

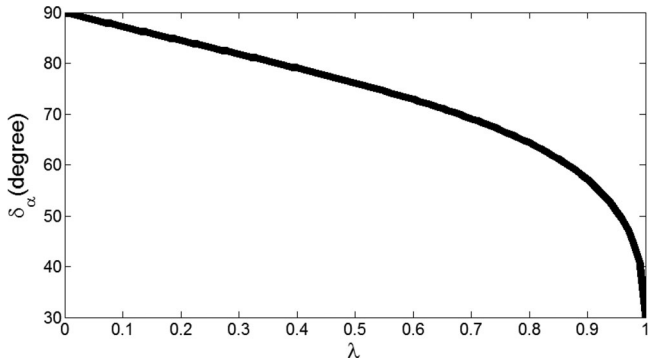


Fig. 4. Curves of $\delta_\alpha(\lambda)$.

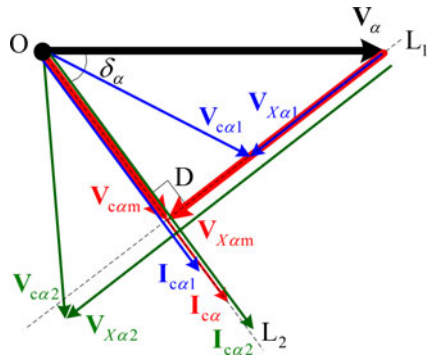


Fig. 5. Phasor diagram of con$\alpha$ when $\delta_\alpha$ is constant.

of $\delta_\alpha$ and $\lambda$ can be obtained as shown in Fig. 4. Obviously, $\delta_\alpha$ is in inverse proportion to $\lambda$.

Besides, the compensating current $I_{c\alpha}$ of con $\alpha$ and load current $I_L$ should satisfy (2), i.e.

$$I_{c\alpha} = \sqrt{I_{c\alpha p}^2 + I_{c\alpha q}^2} = \varepsilon I_L \tag{2}$$

where

$$\varepsilon = \sqrt{-\frac{2}{3}\lambda^2 + \frac{\lambda}{\sqrt{3}}\sqrt{1-\lambda^2} + 1}. \tag{3}$$

### B. Output Voltage of Con$\alpha$

From Fig. 2(a), con$\alpha$'s fundamental output voltage, $V_{c\alpha}$, can be expressed as

$$V_{c\alpha} = V_\alpha + jX_\alpha I_{c\alpha} = f(V_\alpha, X_\alpha, I_{c\alpha}, \delta_\alpha) \tag{4}$$

where $X_\alpha = \omega L_\alpha - 1/\omega C_\alpha$ is the *LC* branch's fundamental reactance of phase-$\alpha$; $\delta_\alpha$ is the phase difference between $\mathbf{V}_\alpha$ and $\mathbf{I}_{c\alpha}$; $f(*)$ represents a function of $V_\alpha$, $X_\alpha$, $I_{c\alpha}$, and $\delta_\alpha$.

For an electric railway supply system, the normal voltage of $V_\alpha$ is a constant, while $X_\alpha$ will be discussed in the next section. So the main task of this part is to discuss the basic relationship among $V_{c\alpha}$, $I_{c\alpha}$, and $\delta_\alpha$.

*1) Situation 1:* The phase of $\mathbf{I}_{c\alpha}$ is constant (i.e., $\delta_\alpha$ unchanging), but its amplitude variable.

Fig. 5 shows the phasor diagram of con$\alpha$'s output voltage ($X_\alpha < 0$) when $\delta_\alpha$ is constant. It can be seen from Fig. 5 that the terminal point of $\mathbf{V}_{c\alpha}$ shifts in the vertical line of $\mathbf{I}_{c\alpha}$ ($\mathbf{V}_{c\alpha 1} \rightarrow \mathbf{V}_{c\alpha m} \rightarrow \mathbf{V}_{c\alpha 2}$) when $\mathbf{I}_{c\alpha}$ varies along with $L_2$ ($\mathbf{I}_{c\alpha 1} \rightarrow \mathbf{I}_{c\alpha} \rightarrow \mathbf{I}_{c\alpha 2}$). The minimum value of $\mathbf{V}_{c\alpha}$, $\mathbf{V}_{c\alpha m}$, precisely appears in the intersection point of $L_1$ and $L_2$ (i.e., point D). So, for every fixed value of $\delta_\alpha$, there is a corresponding $\mathbf{V}_{c\alpha m}$, and it satisfies the following equations:

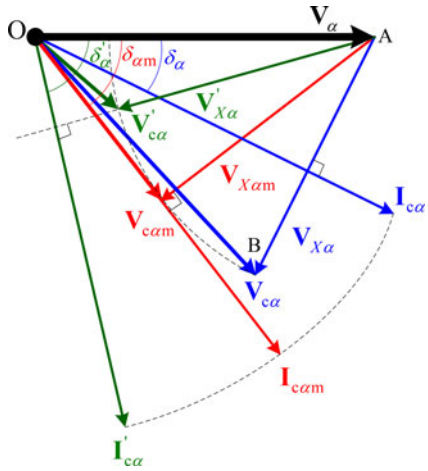


Fig. 6. Phasor diagram of con$\alpha$ when $I_{c\alpha}$ is constant.

$$\begin{cases} \mathbf{V}_{c\alpha m} = V_\alpha \cos\delta_\alpha \\ |X_{\alpha m}| = \frac{1}{\omega C_\alpha} - \omega L_\alpha = \frac{V_\alpha \sin\delta_\alpha}{I_{c\alpha}} \end{cases} \tag{5}$$

where $X_{\alpha m}$ is the *LC* branch's fundamental reactance of phase-$\alpha$ when $\mathbf{V}_{c\alpha} = \mathbf{V}_{c\alpha m}$.

Because $\delta_\alpha \in [30°, 90°]$ (see Fig. 4), it can be calculated from (5) that $\mathbf{V}_{c\alpha m} \in [0, 0.866\mathbf{V}_\alpha]$. That is to say, no matter the changes of $\mathbf{I}_{c\alpha}$'s phasor angle, $\mathbf{V}_{c\alpha m}$ is always less than $\mathbf{V}_\alpha$, and its maximum value is only $0.866\mathbf{V}_\alpha$.

*2) Situation 2:* The amplitude of $\mathbf{I}_{c\alpha}$ is constant, but its phase variable (i.e., $\delta_\alpha$ variable).

Fig. 6 shows the phasor diagram of con$\alpha$ when $\mathbf{I}_{c\alpha}$ is a constant ($X_\alpha = X_{\alpha m} < 0$). The variables shown in Fig. 6 satisfy the following relationship:

$$\begin{cases} I'_{c\alpha} = I_{c\alpha m} = I_{c\alpha} \\ \mathbf{V}'_{X\alpha} = \mathbf{V}_{X\alpha m} = \mathbf{V}_{X\alpha} \\ \delta'_\alpha > \delta_{\alpha m} > \delta_\alpha \\ \mathbf{V}'_{c\alpha} > \mathbf{V}_{c\alpha m} \mathbf{V}_{c\alpha}. \end{cases} \tag{6}$$

It can be seen from Fig. 6 that the smaller the phase angle between $\mathbf{V}_\alpha$ with the compensating current (i.e., $\delta_\alpha < \delta_{\alpha m} < \delta_\alpha$'), the larger the output voltage of con$\alpha$ (i.e., $V_{c\alpha} > V_{c\alpha m} > V_{c\alpha}$'). Because $\delta_\alpha$ is inversely proportional to $\lambda$ (see Fig. 4), it can be concluded from Fig. 6 that when both $I_{c\alpha}$ and $X_\alpha$ are constant, larger $\lambda$ (or smaller $\delta_\alpha$) corresponds to larger $V_{c\alpha}$. Then, the apparent power of con$\alpha$ meets the relationship of $V_{c\alpha}{}' I_{c\alpha}{}' < V_{c\alpha m} I_{c\alpha m} < V_{c\alpha} I_{c\alpha}$.

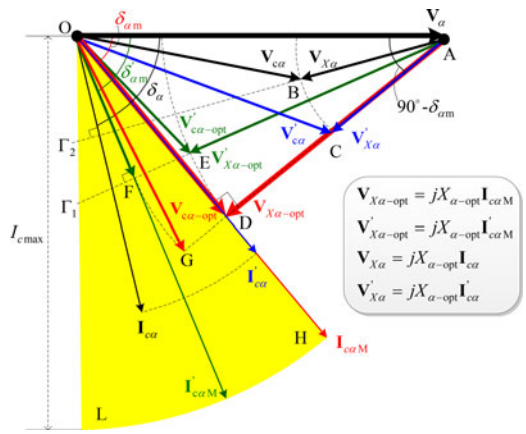


Fig. 7. Phasor diagram of ALC-RPFC in the variable load condition.

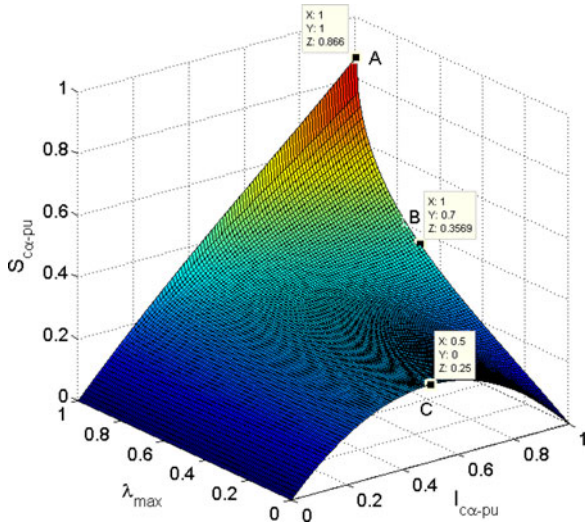


Fig. 8. Relationship among $S_{c\alpha}$, $I_{c\alpha}$, and $\lambda_{\max}$ (Note that the base values are selected as $V_B = V_{\alpha}$, $I_B = I_{c\alpha M}$.).

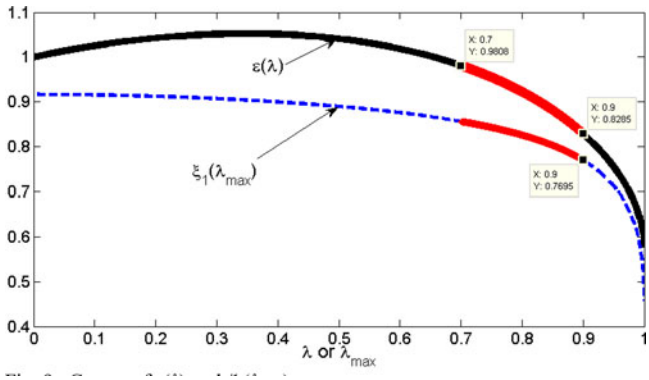


Fig. 9. Curves of $\varepsilon(\lambda)$ and $\xi_1(\lambda_{\max})$.

## IV. Parameter Design and System Control Based on the Fluctuated Load Condition

### A. Parameter Design of Phase-$\alpha$

*1) Synergetic Design Principle Between $\mathbf{X}_{\alpha}$ With Con$\alpha$:* It can be deduced from the previous discussions that $X_{\alpha}$ is a key parameter of ALC-RPFC, which has significant influence for the output performance of the power conditioner. To give an optimal balance between compensating performance and cost-efficiency, we will give a synergetic design guideline for $X_{\alpha}$ and con$\alpha$:

1) When the traction supply system operates in the heavy-load situation, the output voltage of con$\alpha$ should be as low as possible. It allows ALC-RPFC to get the satisfactory heavy-load compensating ability with lower voltage rating and switching frequency. And it also results in higher system reliability and operating efficiency, because the supply system's power quality over-standard and converter faults always occur in the heavy-load situation [14], [31]–[32].
2) In the premise of satisfying the first designing principle, an appropriate $X_{\alpha}$ should also make the apparent power of the converter as high as possible. In this way, the power capacity utilization rate of the compensating system can be increased.
3) In the typical variation range of load currents, the designed $X_{\alpha}$ should make the compensating system to have the obvious economic advantage than conventional RPC.

*2) Designing Idea of $\mathbf{X}_{\alpha}$:*

*a) Realization of the first design principle:* In order to meet the first designing principle, the second term of (5) seems to be an available method. Unfortunately, the load working condition in the real traction network is much complex, so that it is difficult to estimate. It means the parameter design method in static working condition shown in (5) can not be used for real applications. To solve the problem, this part will give a useful one. Its designing idea and practical calculation method will be given in the following statements.

Fig. 7 shows the phasor diagram of ALC-RPFC at four typical working conditions, in which, $\mathbf{I}_{c\alpha}$, $\mathbf{I}_{c\alpha}$', $\mathbf{I}_{c\alpha m}$, and $\mathbf{I}_{c\alpha m}$' are the corresponded four compensating currents of con$\alpha$, and satisfying $I_{c\alpha} = I_{c\alpha}{}' < I_{c\alpha m} = I_{c\alpha m}{}'$. The phase differences between $\mathbf{V}_{\alpha}$ with that four currents are $\delta_{\alpha}$, $\delta_{\alpha m}$, $\delta_{\alpha m}$, and $\delta_{\alpha m}{}'$, respectively. Obviously, $\delta_{\alpha m}$ is the minimum one of them. Considering $\delta_{\alpha} \in [30^{\circ}, 90^{\circ}]$ (see Fig. 4), it can be deduced from Fig. 7 that $30^{\circ} \le \delta_{\alpha m} \le \delta_{\alpha} \le 90$. For discussing convenience, we define $I_{c\alpha m} = I_{c\alpha m}{}' = I_{c\max}$ (see Fig. 7) as the maximal rms-value of the compensating currents; and $\delta_{\alpha m}$ as the minimal angle difference between $\mathbf{V}_{\alpha}$ with con$\alpha$'s compensating currents.

Besides, it can also be observed from Fig. 7 that, $\Delta$ABO, $\Delta$ACO, $\Delta$ADO, and $\Delta$AEO are the voltage phasor triangles of con$\alpha$ corresponding to $\mathbf{I}_{c\alpha}$, $\mathbf{I}_{c\alpha}{}'$, $\mathbf{I}_{c\alpha m}$, and $\mathbf{I}_{c\alpha m}{}'$, respectively. The voltage drops of the *LC* branch in these four cases are $\mathbf{V}_{X\alpha}$, $\mathbf{V}_{X\alpha}{}'$, $\mathbf{V}_{X\alpha\text{-opt}}$, and $\mathbf{V}_{X\alpha\text{ -opt}}{}'$, and their expressions are shown in the lower right corner of Fig. 7 ($X_{\alpha\text{-opt}}$ is the optimal reactance of $X_{\alpha}$, and it will be discussed in the following text).

So, from Fig. 7, it can be concluded that, no matter how the railway load changes, all the compensating currents are located in the yellow fan-shaped area of OHL. Therefore, $\mathbf{I}_{c\alpha}$ and $\mathbf{I}_{c\alpha}{}'$ are the representative compensating currents of con$\alpha$

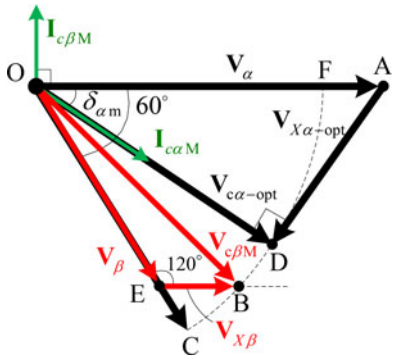


Fig. 10. Phasor diagram of phase-$\beta$.

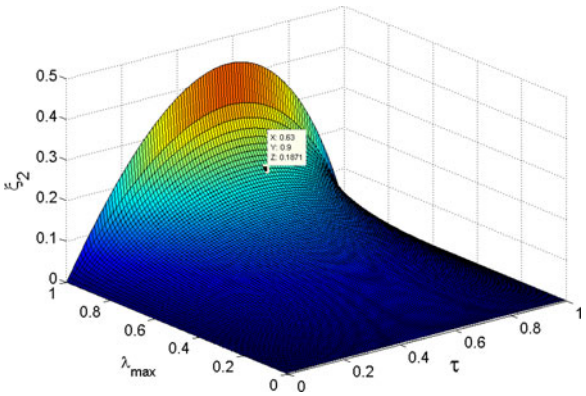


Fig. 11. Design surface of $\xi_2$.

when their amplitudes is less than $I_{c\max}$. While $\mathbf{I}_{c\alpha m}$ and $\mathbf{I}_{c\alpha m}$' are the representative ones when con$\alpha$'s compensating currents is equal to $\mathbf{I}_{c\max}$. Besides, we must emphasize here that the load's PF is not a fixed value in both of those two cases; it changes the value along with $\delta_{\alpha}$.

To ensure the safety of the converters, it is reasonable to select the maximal compensating current as the normal current of con$\alpha$, e.g., $I_{c\alpha m} = I_{c\alpha m}' = I_{c\max}$ should be selected as the normal current. Additionally, when the compensating current equals $I_{c\max}$, a suitable $X_{\alpha}$ should make con$\alpha$ operate at the minimal output voltage, e.g., OD and OF shown in Fig. 7. Because selecting the minimal output voltage as the normal voltage, a minimal apparent power can be obtained. From Fig. 7, it can be observed that $\Delta$ADO and $\Delta$AFO satisfy the condition stated previously, which can be used as the voltage triangle to design $X_{\alpha}$ (Note that $\Delta$AFO is the representative design triangle when the phase of the normal compensating current large than $\delta_{\alpha m}$.).

In the following, we will select an optimal one in those two representative cases: 1) If $\Delta$ADO is adopted to design $X_{\alpha}$, it can be seen from Fig. 7 that when the compensating current changes from the normal current $\mathbf{I}_{c\alpha m}$ to another normal one $\mathbf{I}_{c\alpha m}$', the output voltage of con$\alpha$ will transform from OD to OE. Obviously OE $<$ OD, which means, when the compensating current shifts along with arc HL, adopting $\Delta$ADO to design $X_{\alpha}$, con$\alpha$'s output voltage will not exceed OD. 2) If $\Delta$AFO is adopted to

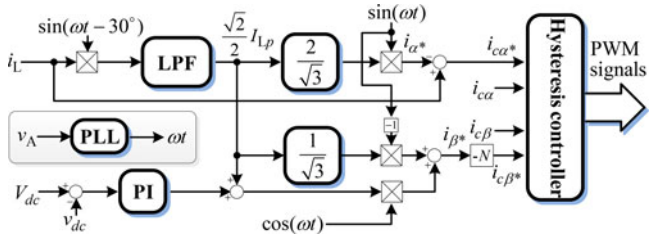


Fig. 12. Control diagram of low-rated ALC-RPFC.

design $X_{\alpha}$, similarly, when the compensating current changes from the normal current $\mathbf{I}_{c\alpha m}$' to another normal current $\mathbf{I}_{c\alpha m}$, the output voltage of con$\alpha$ will transform from OF to OG. Because OG $>$ OD, so con$\alpha$'s apparent power in this situation is larger than that of the $\Delta$ADO-based design method, which has negative influence on converter's initial cost and reliability.

Hence, to get the minimal output voltage and apparent power of con$\alpha$ in the condition of load changes (i.e., the first design principle), select $\Delta$ADO to design $X_{\alpha}$ is better than others. From $\Delta$ADO, the optimal $|X_{\alpha}|, |X_{\alpha-\mathrm{opt}}|$, can be calculated by

$$|X_{\alpha\text{-opt}}| = \frac{\mathrm{AD}}{I_{c\alpha M}} = \frac{V_{X\alpha\text{-opt}}}{I_{c\alpha M}} = \frac{V_{\alpha}\sin\delta_{\alpha m}}{I_{c\alpha M}} \tag{7}$$

where $I_{c\alpha m}$ is the maximum value of $I_{c\alpha}$; $\delta_{\alpha m}$ is the minimum compensating current angle of con$\alpha$, and it satisfies [see (1)]

$$\delta_{\alpha m} = \arctan\left(\frac{1}{\sqrt{3}} + 2\sqrt{\frac{1}{\lambda_{\max}^2} - 1}\right) \tag{8}$$

where $\lambda_{\max}$ is the maximum PF of load current.

*b) Verification of the second design principle:* Referring to Fig. 7, when $I_{c\alpha m}$ (normal current) decreases to $I_{c\alpha}$', $\Delta$ADO degenerates into $\Delta$ACO, and the output voltage of con$\alpha$, however, increases from $V_{c\alpha-\mathrm{opt}}$ (i.e., OD) to $V_{c\alpha}$' (i.e., OC). So, the calculating expression of $X_{\alpha}$, (7), deduced from $\Delta$ADO may not be able to ensure that con$\alpha$ has the maximum apparent power in the condition of load changes. Moreover, all those variables are strongly related to load's PF. So, whether (7) meets the secondary designing principle of $X_{\alpha}$ has to be verified.

Based on the conclusion deduced from Figs. 6, from 7 it can be concluded that the apparent power of con$\alpha$ calculated by $\Delta$ADO and $\Delta$ACO is larger than that of $\Delta$AEO and $\Delta$ABO, respectively. That is to say, the terminal point of $\mathbf{V}_{c\alpha}$ (point B) in $\Delta$ABO (the most ordinary working condition of con$\alpha$) has to be constrained shifting in line AD, can the maximum value of $S_{c\alpha}$ (the apparent power of con$\alpha$) may be obtained. In this case, $\mathbf{I}_{c\alpha} \rightarrow \mathbf{I}_{c\alpha}$', $\Delta$ABO$\rightarrow\Delta$ACO.

From $\Delta$ACO, $S_{c\alpha}$ can be calculated by

$$\begin{aligned} S_{c\alpha} &= I_{c\alpha}\mathbf{V}_{c\alpha}' \\ &= I_{c\alpha}\sqrt{V_{\alpha}^2 + I_{c\alpha}^2 X_{\alpha-\mathrm{opt}}^2 - 2I_{c\alpha}|X_{\alpha-\mathrm{opt}}|V_{\alpha}\sin\delta_{\alpha m}}. \end{aligned} \tag{9}$$

Note that because $\Delta$ABO$\cong\Delta$ACO, $I_{c\alpha}$' is substituted by $I_{c\alpha}$ in (9). Fig. 8 shows the relationship among $S_{c\alpha}$, $I_{c\alpha}$, and $\lambda_{\max}$, which is obtained by the per-unit expression of (9).

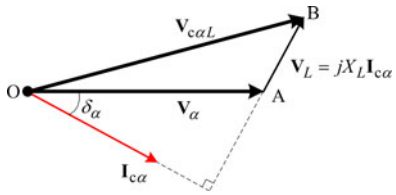


Fig. 13. Phasor diagram of RPC.

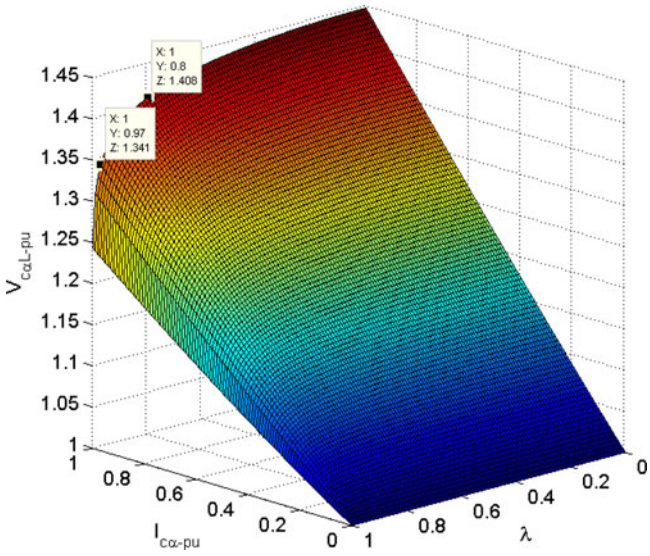


Fig. 14. 3-D plot of $V_{c\alpha L-pu}$ (Note that the base values are $V_B = V_\alpha$, $I_B = I_{c\alpha M}$.).

TABLE I
SPECIFICATIONS OF THE TSS

| Item | Values |
|---|---|
| Grid voltage/short-circuit capacity ($S_d$) | 110 kV ± 5%/530 MVA |
| Type of traction transformer/capacity | V/v transformer/20.5 MVA (phase-$\alpha$:12.5 MVA, Phase-$\beta$:8 MVA) |
| V/v transformer's short-circuit impedance | 10.25% (phase-$\alpha$) 10.67% (phase-$\beta$) |
| Feeder's normal voltage | 27.5 kV |

It can be observed from Fig. 8 that, when $\lambda_{\max} \in [0.7, 1]$ (the typical PF of locomotives), the maximum value of $S_{c\alpha}$ appears exactly when $I_{c\alpha} = 1.0$ p.u. (AB segment). That is to say, for electrical railway loads, the *LC* branch's design method shown in (7) can successfully make $S_{c\alpha}$ reach its maximum value when $\mathbf{I}_{c\alpha} = \mathbf{I}_{c\alpha m}$ [i.e., $\delta_\alpha = \delta_{\alpha m}$ (or $\lambda = \lambda_{max}$) and $I_{c\alpha} = I_{c\alpha m}$]. And it also equals the normal apparent power of con$\alpha$. Therefore, (7) is compatible with the secondary designing principle of $X_\alpha$.

The third designing principle of $X_\alpha$ will be discussed in Section V. By the way, because when $\mathbf{I}_{c\alpha} = \mathbf{I}_{c\alpha m}$, con$\alpha$'s output voltage gets its optimal value ($V_{c\alpha-\text{opt}}$), so we named this method as the optimal voltage design method (OVDM) of $X_\alpha$.

*3) Calculating Method of* $\mathbf{X}_{\alpha-\text{opt}}$ *for Practical Application:* Because $I_{c\alpha}$ cannot be measured directly, (7) is not a convenient calculating method for practical application. The following, we will give a useful one for designing $X_{\alpha-\text{opt}}$.

The curve of $\varepsilon(\lambda)$ is shown in Fig. 9 [originate from (3)]. Usually, the probability of locomotives' PF locates in 0.7∼0.9 is much higher than other values. While, it can be observed from Fig. 9 that when $\lambda \in [0.7, 0.9]$, $\varepsilon(\lambda)$ locates in a narrow interval of 0.8285∼0.9808, which means $I_{c\alpha}$ is approximately proportional with $I_L$. So, referring to (2), $I_{c\alpha m}$ can be approximately expressed as

$$I_{c\alpha M} \approx \frac{I_{\text{LM}}}{0.2}\int_{0.7}^{0.9}\varepsilon(\lambda)d\lambda = \varepsilon_{\text{aver}} I_{\text{LM}} = 0.916 I_{\text{LM}} \quad (10)$$

where $I_{\text{LM}}$ is the maximum value of $I_L$, $\varepsilon_{\text{aver}}$ is the average value of $\varepsilon$ when $\lambda \in [0.7, 0.9]$.

*Remark 1:* For different electrical railway power system, the load's PF may not accurately distributes in 0.7∼0.9, so it is better to modify $\varepsilon_{\text{aver}}$'$s$ value flexibly based on the form shown in (10), by applying the real statistic result of λ in practical applications.

Substituting (10) and (8) into (7), the final practical used expression of $|X_{\alpha-opt}|$ can be expressed as

$$|X_{\alpha-\text{opt}}| = \frac{1}{\omega C_\alpha} - \omega L_\alpha = \xi_1 \frac{V_\alpha}{I_{\text{LM}}} \quad (11)$$

where

$$\xi_1 = \varepsilon_{\text{aver}} \frac{\lambda_{\max}/2\sqrt{3} + \sqrt{1-\lambda_{\max}^2}}{\sqrt{-\frac{2}{3}\lambda_{\max}^2 + \frac{\lambda_{\max}}{\sqrt{3}}\sqrt{1-\lambda_{\max}^2}} + 1}. \quad (12)$$

For the consideration of designing convenience, the curve of $\xi_1(\lambda_{\max})$ is also given in Fig. 9 (dotted line).

The concept of 95%-probability value is always be used in practical cases, so (11) can be also rewritten as

$$|X_{\alpha-\text{opt}}| = \frac{1}{\omega C_\alpha} - \omega L_\alpha = \xi_1|_{\lambda_{\max}=\lambda_{95\%(U)}} \frac{V_\alpha}{I_{L-95\%(U)}} \quad (13)$$

where $\lambda_{95\%(U)}$ and $I_{L-95\%(U)}$ are the upper-95%-probability value of λ and $I_L$, respectively.

Therefore, in the premise of satisfying (12) or (13), $L_\alpha$ and $C_\alpha$ can be configured flexibly according to practical situation (sometimes they are tuned at *n*th harmonics).

## B. Parameter Design of Phase-$\beta$

Fig. 10 shows the phasor diagram of phase-$\beta$, in which, ΔADO is the voltage triangle of con$\alpha$, and it is the same with ΔADO shown in Fig. 7. $\mathbf{I}_{c\beta M}$ is the maximum compensating current phasor of con$\beta$, and it leads $\mathbf{V}_\alpha$ 90°. $\mathbf{V}_{c\beta M}$ is the maximum output voltage of con$\beta$. $\mathbf{V}_\beta$ lags $\mathbf{V}_\alpha$ 60°.

In order to reduce the cost, improve the reliability of converters and design flexibility of the coupling branch, it is reasonable to make $X_\beta$ meet the following design principles:

1) It is better to make $V_{c\beta M} = V_{c\alpha-\text{opt}}$ when the compensating current of con$\alpha$ reaches its maximum value $\mathbf{I}_{c\alpha m}$. This is because it can ensure the operating symmetry of

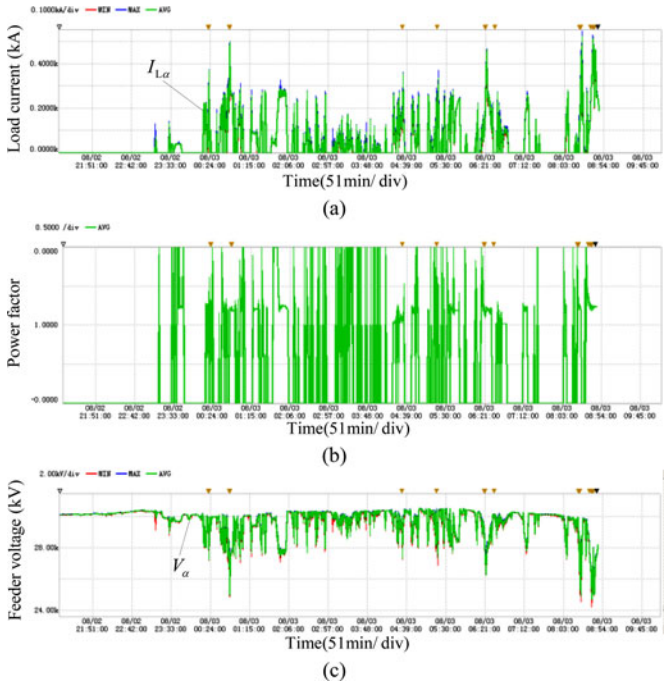


Fig. 15. Phase-$\alpha$'s time-plot waveforms of a real TSS. (a) Load current ($I_{L\alpha}$). (b) Load's PF. (c) Feeder voltage ($V_\alpha$).

con$\alpha$ and con$\beta$, when the whole compensation system works in the severest working condition.

2) In the premise of avoiding large inductance, designers should have sufficient flexibility to match the parameters of coupling branch when $\mathbf{V}_\beta$ is a fixed value (it often happens in the renovation projects). It is convenient for device selection and also helps to reduce the costs and designing difficulties.

To meet the aforementioned designing principles, adopting $L_\beta - C_\beta$ coupling branch is an ideal scheme (Note that $C_\beta$ dominants the branch in fundamental frequency.). Then, the typical voltage triangle of con$\beta$ in Fig. 10 is $\Delta$BEO, where

$$\begin{cases} V_\beta = \mathrm{OE} = \tau V_{c\alpha-opt}, 0 < \tau < 1 \\ V_{X\beta} = \mathrm{EB} = |X_\beta| I_{c\beta M} \\ V_{c\beta M} = \mathrm{OB} = \mathrm{OD} = V_{c\alpha-opt} \end{cases} \tag{14}$$

in which EB is the voltage drop of the *LC*-coupling branch, $X_\beta$ is the fundamental reactance of the *LC* branch of phase-$\beta$.

Besides, $V_\beta$ should be designed less than $V_{c\alpha-\mathrm{opt}}$ (i.e., $V_\beta = \tau V_{c\alpha-\mathrm{opt}}, 0 < \tau < 1$). Referring $\Delta$ADO in Fig. 10, and combine (14) and (7)–(12), it can be calculated that

$$\begin{aligned} V_\beta &= \tau\sqrt{V_\alpha^2 - V_{X\alpha-\mathrm{opt}}^2} \\ &= \frac{\tau\lambda_{\max}}{2\sqrt{-\frac{2}{3}\lambda_{\max}^2 + \frac{\lambda_{\max}}{\sqrt{3}}\sqrt{1-\lambda_{\max}^2}+1}} V_\alpha. \end{aligned} \tag{15}$$

Considering that when $I_{c\beta} = I_{c\beta M}$, the active part of $\mathbf{I}_L$, $I_{Lp}(I_{Lp} = \lambda I_L)$, bound to reach its maximum value, so $I_{c\beta M}$ can be easily calculated by the current relationship shown in Fig. 3, i.e.

$$I_{c\beta M} = \frac{N}{2}\frac{I_{\mathrm{LM}}\lambda_{\max}}{\cos 30^\circ} = N\frac{I_{\mathrm{LM}}\lambda_{\max}}{\sqrt{3}} \tag{16}$$

where $N = V_\alpha / V_\beta$.

By using the cosine theorem in $\Delta$BEO (see Fig. 10) and combining (14)–(16), $|X_\beta|$ can be calculated by

$$|X_\beta| = \frac{1}{\omega C_\beta} - \omega L_\beta = \xi_2 \frac{V_\alpha}{I_{\mathrm{LM}}} \tag{17}$$

where

$$\xi_2 = \frac{\sqrt{3}\tau\left(\sqrt{4-3\tau^2}-\tau\right)\cos^2\delta_{\alpha m}}{2\lambda_{\max}}, 0 < \tau < 1. \tag{18}$$

Similar to design $X_\alpha$, instead of $\lambda_{\max}$ and $I_{\mathrm{LM}}$, $\lambda_{95\%(U)}$ and $I_{L-95\%(U)}$ can also be used in (15) and (17), (18) to calculate $V_\beta$ and $X_\beta$ in practical applications.

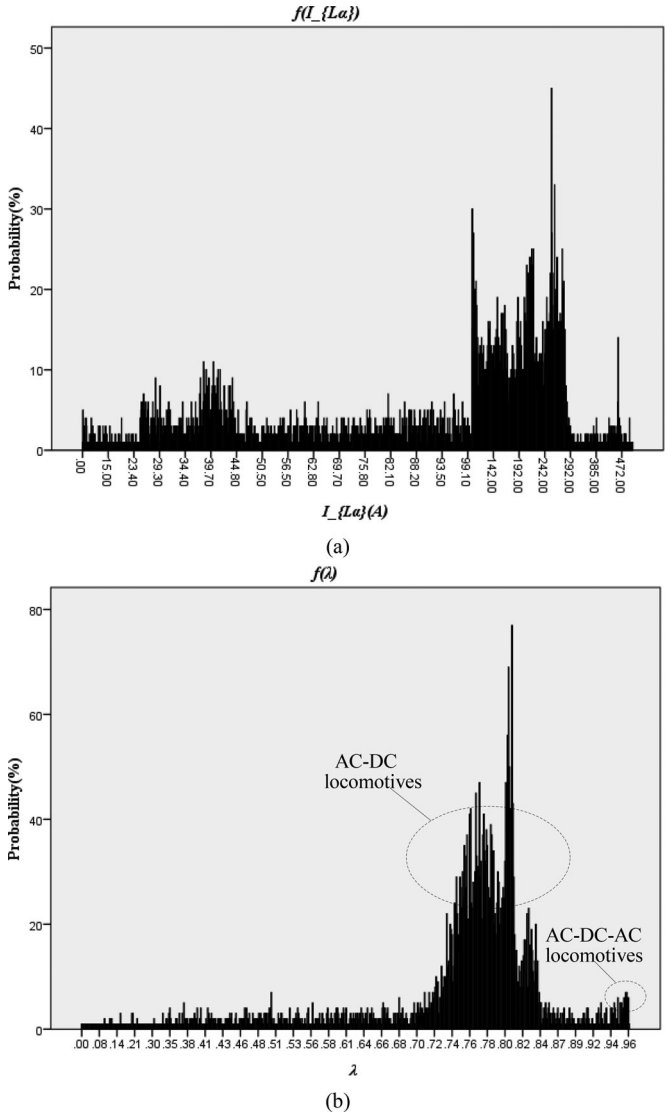


Fig. 16. Probability density curves of $I_{L\alpha}$ and PF. (a) Probability density curves of $I_{L\alpha}$ [i.e., $f(I_{L\alpha})$]. (b) Probability density curves of PF [i.e., $f(\lambda)$].

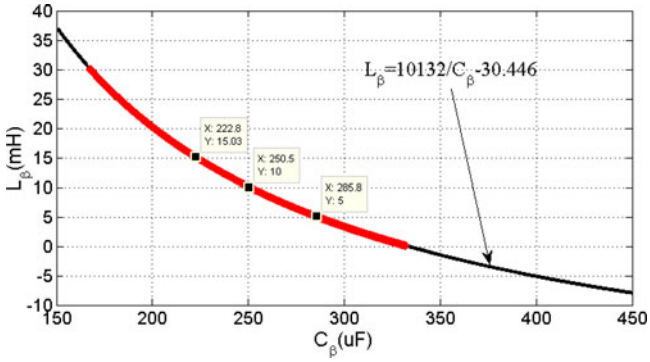


Fig. 17. Designing curve of $L_\beta$ and $C_\beta$.

TABLE II
SIMULATION PARAMETERS OF ALC-RPFC AND RPC*

| $\mathbf{V}_\beta$/kV | $L_\alpha$/mH | $C_\alpha/\mu$F | $L_\beta$/mH | $C_\beta/\mu$F | $L$/mH | $C$/mF |
|---|---|---|---|---|---|---|
| 10 | 6.3 | 65 | 10 | 250 | 45 | 20 |

*$L_\alpha$ and $C_\alpha$ is resonated at fifth harmonics; $C$ is the dc-link capacitance of converters; $L$ is the coupling-inductance of RPC.

The design curve of $L_\beta$ and $C_\beta$ can be easily obtained from (17) and a real design example is shown in Fig. 17 of Section VI, which can be used to flexibly configure $L_\beta$ and $C_\beta$ according to the actual situation. For convenience of design, Fig. 11 gives the design surface of $\xi_2$.

### C. Control System of Low-Rated Laboratory Model

Fig. 12 shows the control diagram of a low-rated ALC-RPFC. Based on the Fourier transformation theory, it can be verified that the output signal of low passive filter is $I_{Lp}/\sqrt{2}$ ($I_{Lp}$ is the active part of $\mathbf{I}_\mathrm{L}$) [17]. $i_{\alpha *}$ and $i_{\beta *}$ are the expected output currents of $\mathrm{T}_\alpha$ and $T_\beta$, respectively. Their phasors are $\mathbf{I}_{\alpha *}$ and $\mathbf{I}_{\beta *}$ in Fig. 3. The signals $i_{c\alpha *}$ and $i_{c\beta *}$ are the references of the compensating currents, which are controlled by a hysteresis controller with the actual compensating currents $i_{c\alpha}$ and $i_{c\beta}$. While, the dc-link voltage is controlled by PI controller and regulated by con$\beta$. This control diagram is also useful for low-rated RPC.

For the consideration of resonance, when the control method shown in Fig. 12 is adopted, ALC-RPFC can be equivalent to an active filter with infinite harmonic damping factor in harmonic frequencies, so the harmonic resonance can be suppressed effectively [29], [30].

## V. POWER CAPACITY ANALYSIS AND DC-LINK VOLTAGE DESIGN

For the same compensating task, ALC-RPFC and RPC have the same compensating currents, so the converters' power ratings of two systems are mainly decided by the output voltage of con$\alpha$ [26], [27]. More accurately to say, is the dc-link voltage.

### A. Proposed ALC-RPFC

It can be observed from $\Delta$ACO in Fig. 7 that, when $\mathbf{I}_{c\alpha}$' increases to $\mathbf{I}_{c\alpha m}$, $\mathbf{V}_{X\alpha}$' $\rightarrow \mathbf{V}_{X\alpha-\mathrm{opt}}$, then con$\alpha$'s output voltage, $V_{c\alpha}$', trends to its minimum value $V_{c\alpha-\mathrm{opt}}$. In addition, it can also be observed from $\Delta$AEO of Fig. 7 that when $\mathbf{I}_{c\alpha m} \rightarrow I_{c\alpha m}$', $\delta_{\alpha m} \rightarrow \delta_{\alpha m}$', which means the PF becomes smaller. Obviously, the output voltage of con$\alpha$, $\mathbf{V}_{c\alpha-opt}$', is less than $V_{c\alpha-\mathrm{opt}}$.

Therefore, it can be concluded that, for a fixed dc-link voltage, the heavier the load or the lower the PF of the locomotive, the better the compensating performance of ALC-RPFC when OVDM is adopted.

In fact, the power quality problems can be neglected when the traction network feeds for light-loaded locomotives with high PF. Because all those NSC or reactive power injected into the utility are attenuated by system's short-circuit capacity. As mentioned previously, since the converter of ALC-RPFC has lower operating voltage in heavy-loaded or low PF situation, so ALC-RPFC is exactly suitable for the heavy-loaded or low PF cases, which has the biggest influence on the utility. This means, the proposed system can meet the power quality requirement of the utility when the dc-link voltage is designed less than the peak value of feeder voltage, i.e., $\sqrt{2}V_\alpha$. Reference to "Appendix A," a satisfactory compensating performance can be obtained when the dc-link voltage of ALC-RPFC is designed within $1.1 \sim 1.35\,\mathbf{V}_\alpha$.

TABLE III
SPECIFICATIONS OF LOAD CURRENTS

| | RMS/A | 1th/A | 3th/A | λ | THD% |
|---|---|---|---|---|---|
| $i_{\alpha L1}$ | 206.4 | 203.0 | 32.4 | 0.805 | 18.19 |
| $i_{\alpha L2}$ | 314.4 | 312.7 | 57.0 | 0.746 | 20.57 |
| $i_{\alpha L1}+i_{\alpha L2}$ | 524.3 | 514.9 | 89.4 | 0.812 | 19.16 |

### B. Conventional RPC

For RPC, the situation is reversed. It can be seen from Fig. 13 that, when $I_{c\alpha}$ increases, the converter's output voltage $V_{c\alpha L}$ of RPC (i.e., OB) will be much larger than $V_\alpha$ (i.e., OA). That is to say, the dc-link voltage of RPC has to be designed much higher than $\sqrt{2}V_\alpha$ when the traction supply system feeds for heavy-load trains. Hence, the voltage rating of power devises along with the initial investment have to be increased, but the system's reliability and operating efficiency decrease consequently.

From Fig. 13, $V_{c\alpha L}$ can be easily obtained from $\Delta$ABO, i.e.

$$V_{c\alpha L} = \sqrt{V_\alpha^2 + I_{c\alpha}^2 X_L^2 + 2I_{c\alpha} X_L V_\alpha \sin\delta_\alpha} \qquad (19)$$

where $X_L$ is the reactance of the coupling inductance of RPC.

Let $X_L = \xi|X_{\alpha-\mathrm{opt}}|$, $(\xi > 0)$, and considering (7), the per-unit form of (19) can be calculated by

$$V_{c\alpha L-pu} = \sqrt{(\xi I_{c\alpha-pu}\sin\delta_{\alpha m})^2 + 2\xi I_{c\alpha-pu}\sin\delta_{\alpha m}\sin\delta_\alpha + 1} \qquad (20)$$

where the subscript "pu" represents the per-unit form of each variable. The base values are selected as $V_B = V_\alpha$, $I_B = I_{c\alpha m}$.

Based on the design experience, $X_L$ is always designed into 18$\sim$25 $\Omega$ when the power rating of RPC's converter reaches 4$\sim$15 MVA [19], [20]. Then $\xi \in [0.45, 0.55]$ (Section VI shows

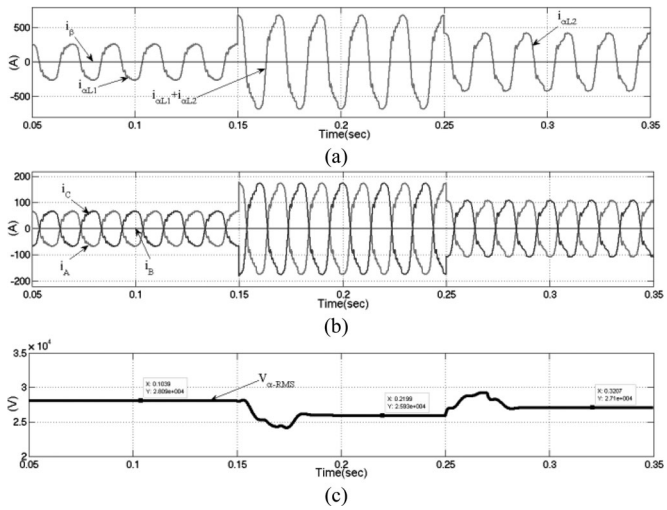


Fig. 18. Simulation waveforms without compensation. (a) Load currents. (b) Primary three phase currents. (c) Feeder voltage's RMS value of phase-$\alpha$.

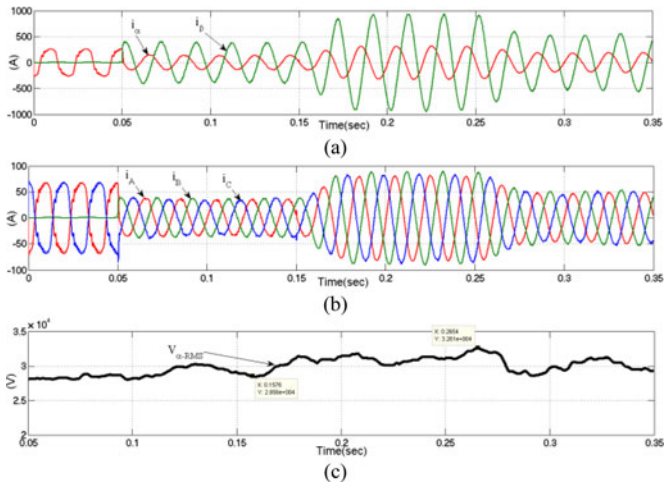


Fig. 20. Simulation waveforms of ALC-RPFC system when $V_{\mathrm{dc\text{-}LC}} = 38.9$ kV. (a) Secondary output currents of main transformer. (b) Primary three phase currents. (c) Feeder voltage's RMS value of phase-$\alpha$.

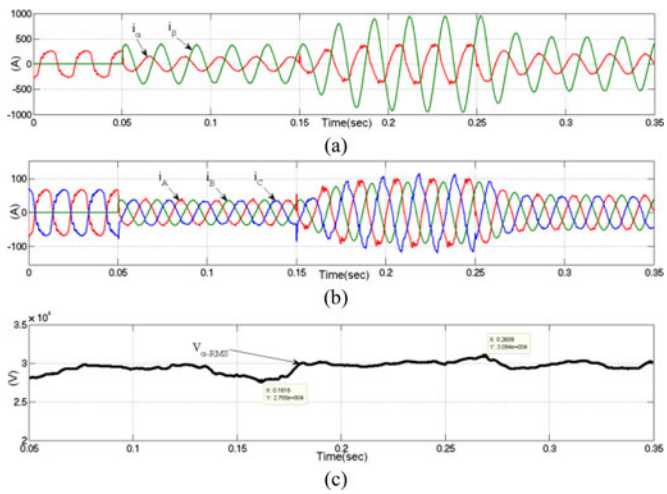


Fig. 19. Simulation waveforms of RPC system when $V_{\mathrm{dc\text{-}}L} = 66.7$ kV. (a) Secondary output currents of main transformer. (b) Primary three phase currents. (c) Feeder voltage's RMS value of phase-$\alpha$.

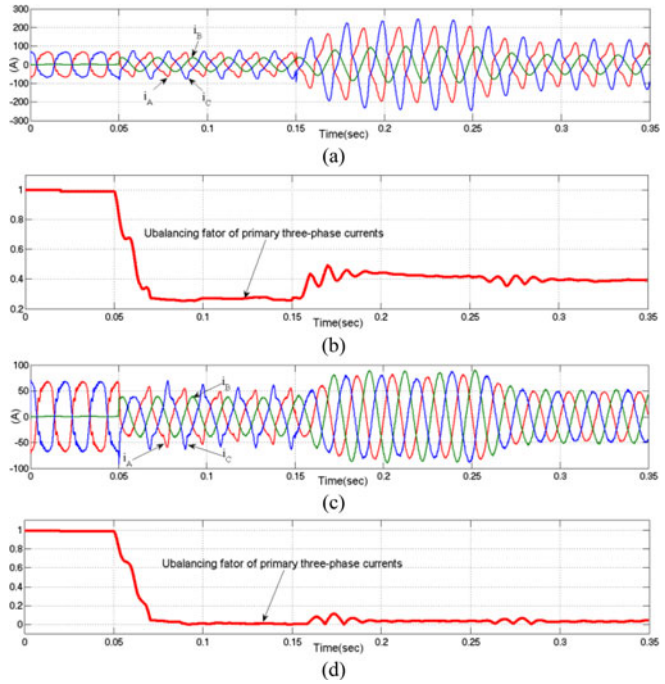


Fig. 21. Simulation waveforms of RPC and ALC-RPFC when the dc-link voltages decrease. (a) Primary three phase currents of RPC when $V_{\mathrm{dc\text{-}}L} = 58$ kV. (b) Unbalance factor of primary three phase currents of RPC system when $V_{\mathrm{dc\text{-}}L} = 58$ kV. (c) Primary three phase currents of ALC-RPFC when $V_{\mathrm{dc-LC}} = 38.3$ kV. (d) Unbalance factor of primary three phase currents of ALC-RPFC system when $V_{\mathrm{dc\text{-}LC}} = 38.3$ kV.

a practical designing example of $X_\alpha$, in which $|X_{\alpha-\mathrm{opt}}| = 46.9\Omega$). Let $\xi = 0.5$ and $\lambda_{\max} = 0.9$ (i.e., $\delta_{\alpha m} = 57.1$, because the probability of PF's upper-95%-probability value of locomotives distributes within 0.85∼0.93 is much higher than other values), the 3-D plot of $\mathbf{V}_{c\alpha L}$ can be obtained from (20), and is shown in Fig. 14.

It can be seen from Fig. 14 that when $\lambda = 0.8$ (the typical PF of ac–dc locomotives) and $I_{c\alpha} = 1.0$ p.u., $V_{c\alpha L}$ reaches its maximum value $1.408V_\alpha$. So the dc-link voltage of RPC $V_{\mathrm{dc}-L}$ has to be designed to the peak value $\sqrt{2}V_{c\alpha L}$ without consideration of harmonics compensation, i.e, $V_{\mathrm{dc}-L} \approx 2V_\alpha$. Compared with the dc-link voltage $V_{\mathrm{dc-LC}} = 1.1 \sim 1.35\ V_\alpha$ of ALC-RPFC, the power rating of RPC increases 32.5%–45%. If the function of active filter is considered, the power rating save ratio of ALC-RPFC will be further increased. On the other hand, considering the locomotive with new generation ac–dc–ac driver system, its PF is always located into 0.96 ∼ 0.97, and without the harmonic pollution. It can be seen from Fig. 14 that the maximum value of $V_{c\alpha L}$ is 1.34 $V_\alpha$. Similarly, $V_{\mathrm{dc}-L}$ should be designed around $1.9\mathrm{V}_\alpha$. So, compared with conventional RPC, the power rating of ALC-RPFC reduces 28.9%–41.8%.

Additionally, referring to $\Delta$ABO in Fig. 13, and considering an extreme situation of RPC, i.e., $X_L \to 0$, $V_{L\alpha} \to 0$, and $V_{c\alpha L} \to V_\alpha$. If $I_{c\alpha} = I_{c\alpha m}$, the normal apparent power of con$\alpha$

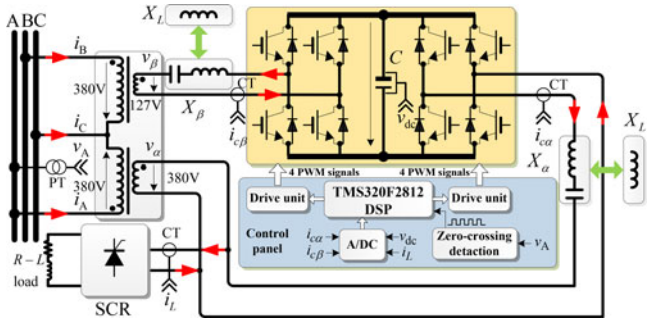


Fig. 22. Experimental wiring diagram.

TABLE IV
EXPERIMENT PARAMETERS*

| $L_\alpha$/mH | $C_\alpha/\mu$F | $L_\beta$/mH | $C_\beta/\mu$F | $L$/mH | $C$/mF | $\mathbf{V}_{\mathrm{dc}\text{-}L/V}$ | $\mathbf{V}_{\mathrm{dc}\text{-}LC/V}$ |
|---|---|---|---|---|---|---|---|
| 5 | 80.5 | 5 | 452 | 10 | 10 | 820 | 490 |

*All the coupling branch parameters are designed based on $\mathbf{I}_{\mathrm{LM}} = 9.8$ A and $\lambda_{\max} = 0.85$. But they are slightly different from the design values because of the practical condition limitation.

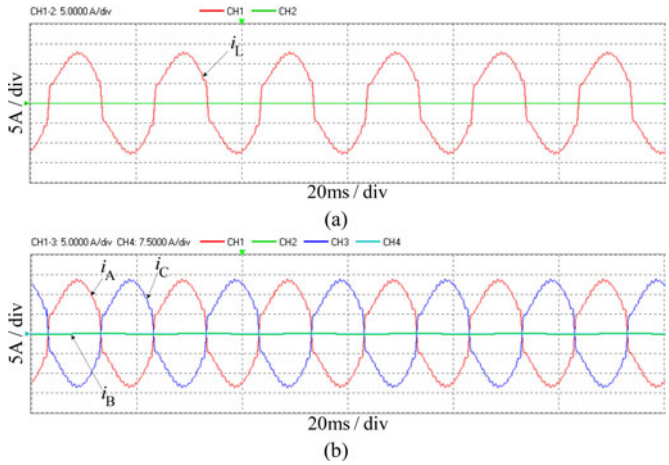


Fig. 23. Current waveforms without compensation. (a) Load currents. (b) Primary three phase currents.

is $\mathrm{V}_\alpha \mathrm{I}_{\mathrm{c}\alpha\mathrm{M}}$ (i.e., 1.0 p.u.). However, it can be obtained from Fig. 8 or (9) that, when $\lambda_{\max} = 0.95$, the maximum apparent power (i.e., the normal apparent power) of ALC-RPC is 0.63 p.u., which means the con$\alpha$'s normal apparent power of ALC-RPC is decreases at least 37% than that of RPC.

When OVDM is adopted, the converter's power rating of ALC-RPFC is much less than that of RPC. Accordingly, the main performance indexes such as initial investment, system reliability, operating efficiency, switching noise, and electromagnetic interference of ALC-RPFC will be better than that of RPC [25], [33], [34]. Where in, the third designing principle of $X_\alpha$ stated in Section IV-A is verified as well.

The underlying difference between ALC-RPFC with RPC is given as follows: The *LC* branch can provide the leading reactive power for feeder, whereas, the L branch of RPC only gives the

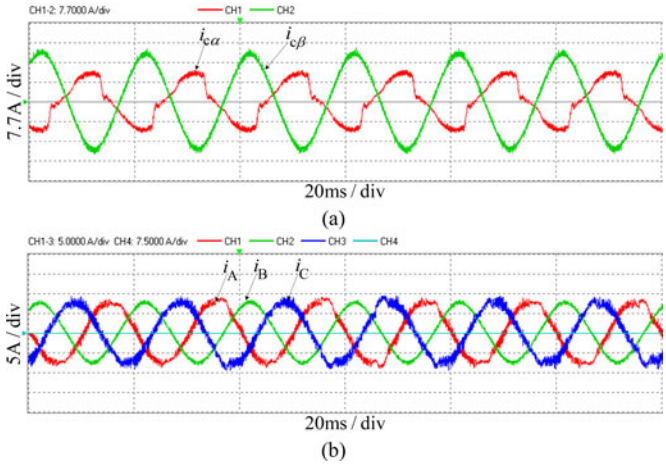


Fig. 24. Steady-state current waveforms of RPC when $V_{\mathrm{dc}\text{-}L} = 820$ V. (a) Compensating currents. (b) Primary three phase currents.

lagging one; so that the voltage drop in *LC* branch (e.g., AD in Fig. 7) lags $\mathbf{V}_\alpha$, while the one in L branch (e.g., AB in Fig. 13) leadings $\mathbf{V}_\alpha$. Hence, for electrical railway loads with the characteristics of lagging reactive power, the converter's output voltage of ALC-RPFC is less than $V_\alpha$ (e.g., OD $<$ OA in Fig. 7); whereas, the converter's output voltage of RPC is large than $V_\alpha$ (e.g., OB $>$ OA in Fig. 13). That is the reason why the power rating of ALC-RPFC is less than that of RPC (Note that for same load, both of them have the same compensating current.).

## VI. SIMULATION AND EXPERIMENT

### A. Simulation

*1) Parameter Design:* Table I shows the specifications of a real TSS. Phase-$\alpha$'s time-plot waveforms and probability density curves of the TSS are shown in Figs. 15 and 16, respectively. It can be seen from Fig. 15 that the load's current and PF of the TSS rapidly changes within $0 \sim 600$A and $0 \sim 1$ respectively [see Fig. 15(a) and (b)], and $V_\alpha$ decreases significantly when the TSS works in the heavy-load situation [see Fig. 15(c)]. All those results indicate that the load variation based designing method proposed in the foregoing sections is important and indispensable.

To get the key parameters of the traction supply system, it is effective to introduce the statistic idea in the designing process of ALC-RPFC. Reference to Fig. 16(a), the load's current, $I_{L\alpha}$, is mainly distributed between 99.1–292 A; both ac–dc locomotives ($\lambda = 0.72 \sim 0.84$) and ac–dc–ac locomotives ($\lambda = 0.94 \sim 0.96$) are supplied by this TSS [see Fig. 16(b)].

From Figs. 15 and 16, we can get the following useful data:

$$\begin{cases} I_{L\alpha-95\%(U)} = 282.6A, I_{L\alpha-95\%(L)} = 110\mathrm{A} \\ \lambda_{95\%(U)} = 0.87, V_\alpha = 29\ k\mathrm{V} \end{cases} \tag{21}$$

where $I_{L\alpha-95\%(U)}$ and $I_{L\alpha-95\%(L)}$ are the upper and lower 95%-probability value of load currents of phase-$\alpha$, respectively.

Considering the load of phase-$\alpha$ will be doubled when the single-phase scheme is adopted, and it needs a designing

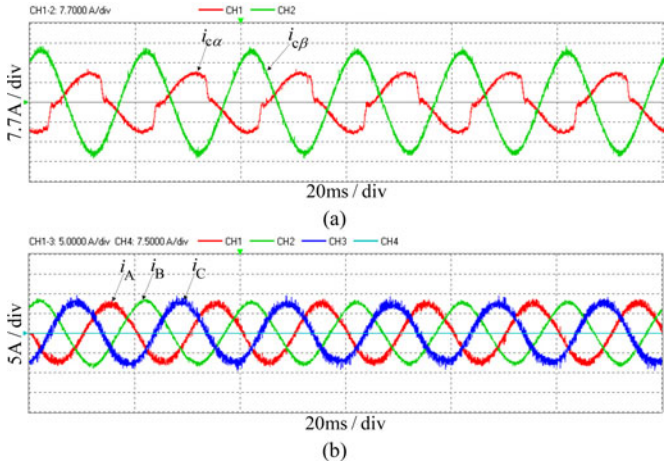


Fig. 25. Steady-state current waveforms of ALC-RPFC when $V_{\mathrm{dc\text{-}LC}} = 490$ V. (a) Compensating currents. (b) Primary three phase currents.

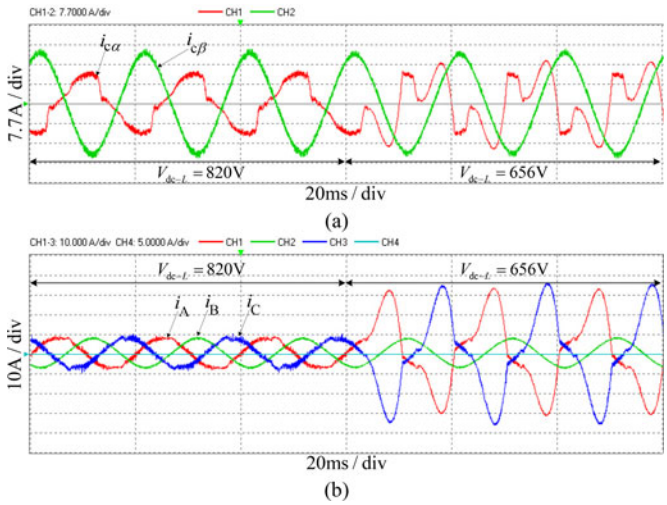


Fig. 26. Dynamic waveforms of RPC when $V_{\mathrm{dc}\text{-}L}$ decreased from 820 to 656 V. (a) Compensating currents. (b) Primary three phase currents.

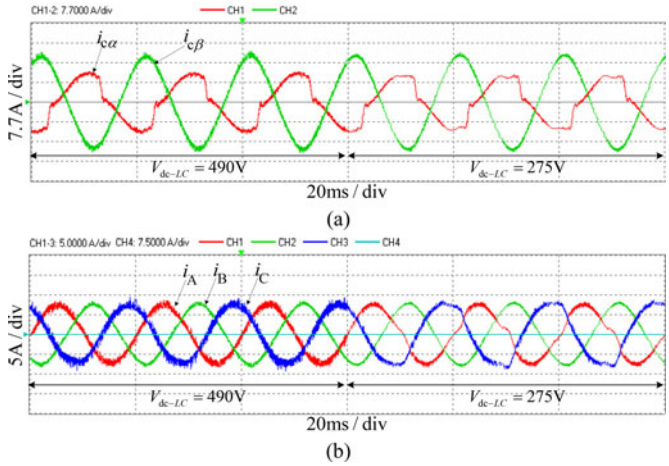


Fig. 27. Dynamic waveforms of ALC-RPFC when $V_{\mathrm{dc\text{-}LC}}$ decreased from 490 to 275 V. (a) Compensating currents. (b) Primary three phase currents.

TABLE V
EXPERIMENT RESULTS IN STEADY STATE

| State | λ | | | THDI/% | | | $\varepsilon_I$/%* |
|---|---|---|---|---|---|---|---|
| | A | B | C | A | B | C | |
| Original state | 0.45 | – | 0.96 | 15.34 | – | 15.51 | 97.72 |
| PRC | 0.97 | 0.99 | 0.98 | 9.30 | 6.10 | 11.21 | 4.84 |
| ALC-RPFC | 0.98 | 0.99 | 0.97 | 7.17 | 5.44 | 7.71 | 5.22 |

*$\varepsilon_I$ is the current unbalancing factor of primary three phase currents.

margin for the compensating system. Then the original designing parameters are selected as

$$\begin{cases} I_{L-95\%(U)} = 2I_{L\alpha-95\%(U)} = 566\,A, I_{L-95\%(L)} \\ \qquad = 2I_{L\alpha-95\%(L)} = 220\,A \\ V_{\mathrm{dc-LC}} = 1.34\,V_{\alpha} = 38.9\,kV, V_{dc-L} = 2.3\,V_{\alpha} \\ \qquad = 66.7\,kV, \lambda_{95\%(U)} = 0.9 \end{cases} \tag{22}$$

where $I_{L-95\%(U)}$ and $I_{L-95\%(L)}$ are the upper and lower 95%-probability value of $I_L$, respectively; $V_{\mathrm{dc-LC}}$ and $V_{\mathrm{dc}-L}$ are the designed dc-link voltage of ALC-RPFC and RPC, respectively.

Based on the discussions stated in Section III-V, other parameters are listed in Table II.

Besides the values shown in Table II, $L_\beta$ and $C_\beta$ can also be configured flexibly from the curve shown in Fig. 17 ($L_\beta > 0$).

*2) Simulation Results:* The specifications of load currents adopted in the simulation are listed in Table III (measured data), in which, $i_{L\alpha 1}$ and $i_{L\alpha 2}$ are adopted to simulate the light (close to $I_{L-95\%(L)}$) and middle-load working conditions of the TSS, respectively. Besides, $i_{L\alpha 1} + i_{L\alpha 2}$ is adopted to simulate the heavy-load situation (close to $I_{L-95\%(U)}$). The simulating waveforms are shown in Figs. 18–21.

Compared with the uncompensated waveforms shown in Fig. 18, it can be observed from Figs. 19 and 20 that the primary three-phase currents are tend to be the sinusoidal waveforms with PF $\approx 1$, and the feed's voltage increases obviously when both systems work in heavy-load situation. It validates the good compensating performance of RPC and ALC-RPFC; although the harmonic compensating performance of RPC is slightly worse than that of ALC-RPFC in the heavy-load case [see Fig. 19 (b)]. However, the power rating of ALC-RPFC is much less than RPC, because $V_{\mathrm{dc-LC}} = 38.9$ kV, which is 58.3% of $V_{\mathrm{dc}\text{-}L}\,(66.7\,\mathrm{kV})$.

It can be seen from Fig. 21(a) and (b) that, the conventional RPC shows a worse heavy-load compensating performance when $V_{\mathrm{dc}\text{-}L}$ decreases 13% (i.e., $V_{\mathrm{dc}\text{-}L} = 58$ kV). However, when $V_{\mathrm{dc\text{-}LC}}$ decreases from 38.9 to 38.3 kV, ALC-RPFC's compensating performance is almost unchanged in heavy-load working condition [see Fig. 21(c) and (d)]. Except that a small amount of harmonics are not eliminated completely in light-load working condition (in fact, they are attenuated by $S_d$). This shows that the heavy-load compensating performance of ALC-RPFC is much better than that of RPC.

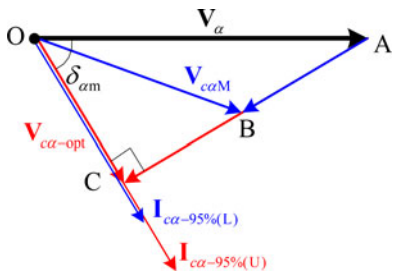


Fig. 28. Phasor diagram of con$\alpha$ when OVDM is adopted.

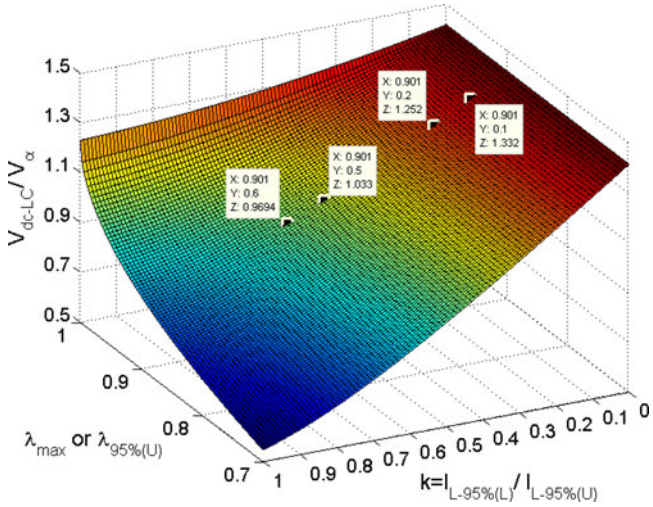


Fig. 29. Relationship among $V_{\mathrm{dc\text{-}LC}}/V_{\alpha}$, $k$, and $\lambda_{\max}(or\lambda_{95\%(U)})$.

### *B. Experiment*

For further validation of the proposed system, the physical platforms of RPC and ALC-RPFC have been built in a laboratory. The wiring diagram of this setup is shown in Fig. 22. The power rating of the main transformer with turn ratio of 380 V: 380 V and 380 V: 127 V is 40 kVA. The SCR-controlled *RL* load is adopted to simulate the locomotive with the normal apparent power of 3.8 kVA and PF $\approx$ 0.85.

Four voltage and current signals through A/D converter are measured as the input of TMS320F2812 DSP. $v_A$ provides the synchronous signal for the whole control system. The detection and control algorithms mentioned in Section IV-C are carried out in DSP for digital implementation. The event manager of the DSP emits eight PWM signals through the driver unit as the control signal for two H-bridge converters. Besides, the sample frequency is selected as 12.8 kHz, the scale of IGBT is 1200 V/450 A. Other experiment parameters are listed in Table IV; HIOKI-3196 power quality analyzer is used for data acquisition. The experiment results are shown in Figs. 23–27 and Table V.

The current waveforms of RPC and ALC-RPFC are shown in Figs. 24 and 25, respectively, their experimental data are listed in Table V. Compared with the uncompensated waveforms shown in Fig. 23, the results shown in Figs. 24 and 25 further verify the satisfactory compensating performance of RPC and ALC-RPFC; however, $V_{\mathrm{dc\text{-}LC}} = 490$ V, which is 59.8% of $V_{\mathrm{dc}\text{-}L}$ (820 V). The result further validates the good power rating saving ability of ALC-RPFC.

In addition, it can be seen from the dynamic waveforms shown in Figs. 26 and 27, that if the dc-link voltage of RPC decreases by 20% to 656 V (it is still larger than the feeder's peak voltage $380\sqrt{2}$ V), the compensating performance turns bad (see Fig. 26). However, it can be seen from Fig. 27, that when the dc-link voltage of ALC-RPFC decreases from 490 to 275 V (reducing ratio is 44%), the compensating performance of ALC-RPFC almost unchange. If the load current in experimental situation corresponds to the heaviest working condition of a traction network (i.e., $I_{\mathrm{LM}} = 9.8$ A, $\lambda_{\max} = 0.85$), the aforementioned experiment results also indicate that the power quality problems in most heavy-load cases can be compensated by ALC-RPFC when $V_{\mathrm{dc-LC}}$ is designed at 490 V. Also, the dynamic results further validate the effectiveness of the ALC-RPC's ability on decreasing the power capacity.

## VII. Conclusion

This paper proposed an asymmetric double *LC*-coupled railway power conditioner for single-phase ac electric railway supply system. At first, its operating property under fluctuated load condition is analyzed in detail. To meet the demand of practical applications for the "intense and random" load of electrical railway power system, we proposed a systematic design method for *LC*-coupling branches, and the corresponded power capacity analysis method for the purpose of determining the design range of ALC-RPFC's dc-link voltage. Finally, simulation and experiment results validate these conceptions.

ALC-RPFC fully explores the potentials of two asymmetric passive *LC* branches. In comparison to conventional RPC, it has excellent heavy-load compensating ability with lower dc-link voltage. Besides, all the parameters' design methods proposed in this paper are based on the fluctuated electrical railway working condition, and they are also useful for industrial applications. Therefore, the proposed conditioner is an industrial effective electric railway compensating system with high cost-efficiency and high reliability.

## Appendix A

Fig. 28 shows the phasor diagram of con$\alpha$ when OVDM is adopted. In Fig. 28, AB and AC is the minimum and maximum voltage drop of $X_{\alpha-\mathrm{opt}}$, respectively, and satisfying

$$\begin{cases} \mathrm{AB} = |X_{\alpha\text{-opt}}|I_{c\alpha\text{-}95\%(\mathrm{L})} \approx |X_{\alpha\text{-opt}}|\varepsilon_{\mathrm{aver}} I_{L\text{-}95\%(\mathrm{L})} \\ \mathrm{AC} = |X_{\alpha\text{-opt}}|I_{c\alpha\text{-}95\%(\mathrm{U})} \approx |X_{\alpha\text{-opt}}|\varepsilon_{\mathrm{aver}} I_{L\text{-}95\%(\mathrm{U})} \end{cases} \tag{A1}$$

where $I_{c\alpha\text{-}95\%(U)}$, $I_{c\alpha\text{-}95\%(L)}$ and $I_{L\text{-}95\%(U)}$, $I_{L\text{-}95\%(L)}$ are the upper and lower 95%-probability value of $I_{c\alpha}$ and $I_L$, respectively.

From Fig. 28, $\mathbf{V}_{c\alpha m}$ is the maximum output voltage of con$\alpha$. By using the cosine theorem in $\Delta$ABO and combining (13), $V_{c\alpha m}$ can be calculated as

$$V_{c\alpha\mathrm{M}} = V_\alpha \sqrt{\varepsilon_{\mathrm{aver}}^2 \xi_1^2 k^2 - 2\varepsilon_{\mathrm{aver}} \xi_1 k \sin\delta_{\alpha\mathrm{m}} + 1} \qquad \text{(A2)}$$

where $k = I_{L-95\%(L)}/I_{L-95\%(U)}$.

Considering the designed dc-link voltage of ALC-RPFC $V_{\mathrm{dc-LC}}$ should satisfy

$$V_{\mathrm{dc\ -LC}} = \sqrt{2} V_{c\alpha\mathrm{M}}. \qquad \text{(A3)}$$

Combining (A.2), (A.3), and (12), we can obtain Fig. 29.

In practical situation, $k$ and $\lambda_{\max}$ (or $\lambda_{95\%(U)}$) are always located in $0.2 \sim 0.5$ and $0.85 \sim 0.93$, respectively. It can be seen from Fig. 29 that, a good compensating performance can be obtained when the designed dc-link voltage of ALC-RPFC is selected as $1.1 \sim 1.35\, V_\alpha$.

## REFERENCES


[1] Z. He, H. Hu, Y. Zhang, and S. Gao, "Harmonic resonance assessment to traction power-supply system considering train model in china high-speed railway," *IEEE Trans. Power Del.*, vol. 29, no. 4, pp. 1735–1743, Aug. 2014.

[2] S. L. Chen, R. J. Li, and H. Pao-Hsiang, "Traction system unbalance problem-analysis methodologies," *IEEE Trans. Power Del.*, vol. 19, no. 4, pp. 1877–1883, Oct. 2004.

[3] E. Pilo de la Fuente, S. K. Mazumder, and I. Gonzalez Franco, "Railway electrical smart grids: An introduction to next-generation railway power systems and their operation," *IEEE. Electrification Mag.*, vol. 2, no. 8, pp. 49–55, Sep. 2014.

[4] T. Kneschke, "Control of utility system unbalance caused by single-phase electric traction," *IEEE Trans. Ind. Appl.*, vol. IA-21, no. 6, pp. 1559–1570, Nov. 1985.

[5] Z. Zhang, B. Wu, J. Kang, and L. Luo, "A multi-purpose balanced transformer for railway traction applications," *IEEE Trans. Power Del.*, vol. 24, no. 2, pp. 711–718, Apr. 2009.

[6] H. Morimoto, T. Uzuka, A. Horiguchi, and T. Akita, "New type of feeding transformer for AC railway traction system," in *Proc. Int. Power Electron. Drive Syst. Conf.*, 2009, pp. 800–805.

[7] S.V. Raygani, A. Tahavorgar, S.S. Fazel, and B. Moaveni, "Load flow analysis and future development study for an AC electric railway," *IET Elect. Syst. Transportation*, vol. 2, no. 3, pp. 139–147, Sep. 2012.

[8] X. He, Z. Shu, X. Peng, Q. Zhou, Y. Zhou, Q. J. Zhou, and S. Gao, "Advanced cophase traction power supply system based on three-phase to single-phase converter," *IEEE Trans. Power Electron.*, vol. 29, no. 10, pp. 5323–5333, Oct. 2014.

[9] S. Hu, Z. Zhang, Y. Li, L. Luo, Y. Cao, and C. Rehtanz, "A new half-bridge winding compensation based power conditioning system for electric railway with LQRI," *IEEE Trans. Power Electron.*, vol. 29, no. 10, pp. 5242–5256, Oct. 2014.

[10] A.Bueno, J. Aller, J. Restrepo, R. Harley, and T. Habetler, "Harmonic and unbalance compensation based on direct power control for electric railway systems," *IEEE Trans. Power Electron.*, vol. 28, no. 12, pp. 5823–5831, Dec. 2013.

[11] K. Kunomura, M. Onishi, M. Kai, N. Iio, M. Otsuki, Y. Tsuruma, and N. Nakajima, "Electronic frequency converter feeding single-phase circuit and controlling feeder voltage with fixed power factor method for shinkansen," *IEEE Trans. Power Electron.*, vol. 27, no. 9, pp. 3888–3896, Sep. 2012.

[12] S. Senini and P. Wolfs, "Hybrid active filter for harmonically unbalanced three phase three wire railway traction loads," *IEEE Trans. Power Electron.*, vol. 15, no. 4, pp. 702–710, Jul. 2000.

[13] P. Tan, P. Loh, and D. Holmes, "Optimal impedance termination of 25-kV electrified railway systems for improved power quality," *IEEE Trans. Power Del.*, vol. 20, no. 2, pp. 1703–1710, Apr. 2005.

[14] G. Raimondo, P. Ladoux, A. Lowinsky, H. Caron, and P. Marino, "Reactive power compensation in railways based on AC boost choppers," *IET Elect. Syst. Transportation*, vol. 2, no. 4, pp. 169–177, Dec. 2012.

[15] P. Ladoux, G. Raimondo, H. Caron, and P. Marino, "Chopper-controlled steinmetz circuit for voltage balancing in railway substations," *IEEE Trans. Power Electron.*, vol. 28, no. 12, pp. 5813–5822, Dec. 2013.

[16] B. Bahrani and A. Rufer, "Optimization-based voltage support in traction networks using active line-side converters," *IEEE Trans. Power Electron.*, vol. 28, no. 2, pp. 673–685, Feb. 2013.

[17] A. Luo, C. Wu, J. Shen, Z. Shuai, and F. Ma, "Railway static power conditioners for high-speed train traction power supply systems using three-phase V/v transformers," *IEEE Trans. Power Electron.*, vol. 26, no. 10, pp. 2844–2856, Oct. 2011.

[18] Z. Shu, S. Xie, K. Lu, Y. Zhao, X. Nan, D. Qiu, F. Zhou, S. Gao, and Q. Li, "Digital detection, control, and distribution system for co-phase traction power supply application," *IEEE Trans. Ind. Electron.*, vol. 60, no. 5, pp. 1831–1839, May 2013.

[19] T. Uzuka, S. Ikedo, K. Ueda, Y. Mochinaga, S. Funahashi, and K. Ide, "Voltage fluctuation compensator for shinkansen," *IEEE J. Trans. Power Energy*, vol. 162, no. 4, pp. 25–33, Sep. 2008.

[20] O. Masataro and Y. Yasuhiro, "Validation of railway static power conditioner in Tohoku Shinkansen on actual operation," in *Proc. Int. Power Electron. Conf.*, 2010, pp. 2160–2164.

[21] K. Lao, N. Dai, W. Liu, and M. Wong, "Hybrid power quality compensator with minimum dc operation voltage design for high-speed traction power systems," *IEEE Trans. Power Electron.*, vol. 28, no. 4, pp. 2024–2036, Apr. 2013.

[22] S. Rahmani, A. Hamadi, N. Mendalek, and K. Al-Haddad, "A new control technique for three-phase shunt hybrid power filter," *IEEE Trans. Ind. Electron.*, vol. 56, no. 8, pp. 2904–2915, Aug. 2009.

[23] A. Bhattacharya, C. Chakraborty, and S. Bhattacharya, "Parallel-connected shunt hybrid active power filters operating at different switching frequencies for improved performance," *IEEE Trans. Ind. Electron.*, vol. 59, no. 11, pp. 4007–4019, Nov. 2012.

[24] Y. Li, T. Saha, O. Krause, Y. Cao, and C. Rehtanz, "An inductively active filtering method for power-quality improvement of distribution networks with nonlinear loads," *IEEE Trans. Power Del.*, vol. 28, no. 4, pp. 2465–2473, Oct. 2013.

[25] A. F. Zobaa, "Optimal multiobjective design of hybrid active power filters considering a distorted environment," *IEEE Trans. Ind. Electron.*, vol. 61, no. 1, pp. 107–114, Jan. 2014.

[26] S. Karanki, N. Geddada, M. Mishra, and B. Kumar, "A modified three-phase four-wire UPQC topology with reduced dc-link voltage rating," *IEEE Trans. Ind. Electron.*, vol. 60, no. 9, pp. 3555–3566, Sep. 2013.

[27] M. I. Montero, E. R. Cadaval, and F. B. González, "Hybrid multiconverter conditioner topology for high-power applications," *IEEE Trans. Ind. Electron.*, vol. 58, no. 6, pp. 2283–2292, Jun. 2011.

[28] S. Kouro, M. Malinowski, K. Gopakumar, J. Pou, L. G. Franquelo, B. Wu, J. Rodriguez, M. A. Pérez, and J. I. Leon, "Recent advances and industrial applications of multilevel converters," *IEEE Trans. Ind. Electron.*, vol. 57, no. 8, pp. 2553–2580, Aug. 2010.

[29] S. Srianthumrong and H. Akagi, "A medium-voltage transformerless ac/dc power conversion system consisting of a diode rectifier and a shunt active filter," *IEEE Trans. Ind. Appl.*, vol. 39, no. 3, pp. 874–882, May 2003.

[30] C. Lam, W. Choi, M. Wong, and Y. Han, "Adaptive dc-Link voltage-controlled hybrid active power filters for reactive power compensation," *IEEE Trans. Power Electron.*, vol. 27, no. 4, pp. 1758–1772, Apr. 2012.

[31] F. Richardeau and T. Pham, "Reliability calculation of multilevel converters: Theory and applications," *IEEE Trans. Ind. Electron.*, vol. 60, no. 10, pp. 4225–4233, Oct. 2013.

[32] X. Perpiñà, X. Jordà, M. Vellvehi, J. Rebollo, and M. Guyennet, "Long-term reliability of railway power inverters cooled by heat-pipe-based systems," *IEEE Trans. Ind. Electron.*, vol. 58, no. 7, pp. 2662–2672, Jul. 2011.

[33] F. Casanellas, "Losses in PWM inverters using IGBTs," *Proc. Inst. Elect. Eng.*, vol. 141, pp. 235–239, Sep. 1994.

[34] Q. Liu, W. Shen, D. Boroyevich, V. Stefanovic, and M. Arpilliere, "Experimental evaluation of IGBTs for characterizing and modeling conducted EMI emission in PWM inverters," in *Proc. Power Electron. Spec. Conf.*, 2003, pp. 1951–1956.

**Sijia Hu** (S'14) was born in Hunan, China, in 1987. He received the B.Sc. degree in 2010. Since 2012, he has been working toward the Ph.D. degree at the College of Electrical and Information Engineering, Hunan University, Changsha, China.

His research interests include power flow control and power quality analysis and control of electric railway power system, high-power converters, and FACTS technologies. In recent years, he has been a key member of the NSFC Support Programs under Grants 51477046, 51077044, and 51377001 and the Hunan Provincial for Key Scientific and Technological Projects under Grant 12JJ2034.

**Zhiwen Zhang** received the B.Sc. and M.Sc. degrees in electrical engineering and the Ph.D. degree in control theory and control engineering from Hunan University, Changsha, China.

He was a Visiting Scholar at Tsinghua University, Beijing, China, and a Visiting Professor at Ryerson University, Toronto, ON, Canada.

He is currently a Full Professor at the College of Electrical and Information Engineering, Hunan University. His research interests include power quality analysis and control of electric railway power system, theory and new technology of ac/dc energy transform, theory and application of new-type electric apparatus, harmonic suppression for electric railway, power electronics application, and computer control.

**Yong Li** (S'09–M'12–SM'14) was born in Henan, China, in 1982. He received the B.Sc. and Ph.D. degrees in 2004 and 2011, respectively, from the College of Electrical and Information Engineering, Hunan University, Changsha, China. He received the second Ph.D. degree in June 2012 from the Institute of Energy Systems, Energy Efficiency, and Energy Economics, TU Dortmund University, Dortmund, Germany.

Since 2009, he worked as a Research Associate at the Institute of Energy Systems, Energy Efficiency, and Energy Economics, TU Dortmund University. After that, he was a Research Fellow with the University of Queensland, Brisbane, Australia. Since 2014, he has been a Full Professor of electrical engineering at Hunan University. His current research interests include power system stability analysis and control, ac/dc energy conversion systems and equipment, analysis and control of power quality, and HVDC and FACTS technologies.

Dr. Li is a Member of the Association for Electrical, Electronic and Information Technologies, Germany.

**Longfu Luo** (M'09) was born in Hunan, China, in 1962. He received the B.Sc., M.Sc., and Ph.D. degrees from the College of Electrical and Information Engineering, Hunan University, Changsha, China, in 1983, 1991, and 2001, respectively.

From 2001 to 2002, he was a Senior Visiting Scholar at the University of Regina, Regina, SK, Canada. He is currently a Full Professor of electrical engineering at the College of Electrical and Information Engineering, Hunan University. His current research interests include the design and optimization of modern electrical equipment, the development of new converter transformer, and the study of corresponding new HVDC theories.

**Pei Luo** was born in Hunan, China, in 1974. He received the B.Sc. and M.Sc. degrees from the College of Information Engineering, Xiangtan University, Xiangtan, China, in 1996 and 2006, respectively. He is working toward the Ph.D. degree at the College of Electrical and Information Engineering, Hunan University, Changsha, China.

He is currently a Duty Professor at the College of Information Engineering, Xiangtan University. His research interests include power flow control and power quality analysis and control of electric railway power system, reactive power compensation, and active power filters.

**Yijia Cao** (M'98–SM'13) was born in Hunan, China, in 1969. He received the Graduation degree from Xi'an Jiaotong University, Xi'an, China, in 1988, and received the M.Sc. and Ph.D. degrees from the Huazhong University of Science and Technology (HUST), Wuhan, China, in 1991 and 1994, respectively.

From September 1994 to April 2000, he worked as a Visiting Research Fellow and Research Fellow at Loughborough University, Liverpool University, and the University of West England. From 2000 to 2001, he was a Full Professor at HUST, and from 2001 to 2008, he was a Full Professor at Zhejiang University. He was appointed as a Deputy Dean of the College of Electrical Engineering, Zhejiang University, in 2005. He is currently a Full Professor and the Vice President of Hunan University, Changsha, China. His research interests include power system stability control and the application of intelligent systems in power systems.

**Yuehui Chen** was born in Hunan, China, in 1965. He received the Ph.D. degree from the Huazhong University of Science and Technology, Wuhan, China, in 2012.

He is currently a Deputy Chief Engineer at State Grid Hunan Electric Power Company, Changsha, China. His research interests include power system planning, management of power grid, and power quality analysis and control.

**Guandong Zhou** was born in Hunan, China, in 1965. He received the M.Sc. degree from Hunan University, Changsha, China, in 1991.

He is currently a Director at the Science and Technology Department of Environmental Protection, State Grid Hunan Electric Power Company, Changsha, China. His research interests include power system stability analysis and control, grid security and economic operation, and power quality analysis and control.

**Bin Wu** (S'89–M'92–SM'99–F'08) received the Ph.D. degree in electrical and computer engineering from the University of Toronto, Toronto, ON, Canada, in 1993.

After being with Rockwell Automation, Canada, as a Senior Engineer, he joined Ryerson University, Toronto, ON, Canada, where he is currently a Professor and NSERC/Rockwell Industrial Research Chair in power electronics and electric drives. He has published more than 280 technical papers, authored/coauthored two Wiley-IEEE Press books, and holds more than 20 issued/pending patents in the area of power conversion, advanced controls, adjustable-speed drives, and renewable energy systems.

Dr. Wu received the Gold Medal of the Governor General of Canada, the Premiers Research Excellence Award, Ryerson Distinguished Scholar Award, Ryerson Research Chair Award, and the NSERC Synergy Award for Innovation. He is a Fellow of the Engineering Institute of Canada and the Canadian Academy of Engineering.

**Christian Rehtanz** (M'96–SM'06) was born in Germany in 1968. He received the Diploma and Ph.D. degrees in 1994 and 1997, respectively, from the TU Dortmund University, Dortmund, Germany. In 2003, he received the *Venia Legendi* in electrical power systems from the Swiss Federal Institute of Technology, Zurich, Switzerland.

In 2000, he joined ABB Corporate Research, Switzerland. He became the Head of technology for the global ABB business area of power systems in 2003, and the Director of ABB Corporate Research, China, in 2005. Since 2007, he has been the Head of the Institute of Energy Systems, Energy Efficiency and Energy Economics, TU Dortmund University. In addition, he has been a Scientific Advisor of ef.Ruhr GmbH since 2007. He is an Adjunct Professor at the Hunan University, Changsha, China. His research interests include electrical power systems and power economics including technologies for network enhancement and congestion relief like stability assessment, wide-area monitoring, protection, and coordinated network-control as well as integration and control of distributed generation and storages. He is the author of more than 150 scientific publications, three books, and 17 patents and patent applications.

Dr. Rehtanz received the MIT World Top 100 Young Innovators Award in 2003.